Identification of key residues involved in Si transport by the aquaglyceroporins

Gabriel A. Carpentier, Alexandre P. Garneau, Andrée-Anne Marcoux, Micheline Noël, Rachelle Frenette-Cotton, and Paul Isenring

Nephrology Research Group, Department of Medicine, Laval University, L'Hôtel-Dieu de Québec Hospital, Québec, Québec G1R 2J6, Canada

We recently demonstrated that the aquaglyceroporins (AQGPs) could act as potent transporters for orthosilicic acid (H_4SiO_4). Although interesting, this finding raised the question of whether water and H_4SiO_4, the transportable form of Si, permeate AQGPs by interacting with the same region of the pore, especially in view of the difference in molecular radius between the two substrates. Here, our goal was to identify residues that endow the AQGPs with the ability to facilitate Si diffusion by examining the transport characteristics of mutants in which residues were interchanged between a water-permeable but Si-impermeable channel (aquaporin 1 [AQP1]) and a Si-permeable but water-impermeable channel (AQP10). Our results indicate that the composition of the arginine filter (XX/R), known to include three residues that play an important role in water transport, may also be involved in Si selectivity. Interchanging the identities of the nonarginine residues within this filter causes Si transport to increase by approximately sevenfold in AQP1 and to decrease by approximately threefold in AQP10, whereas water transport and channel expression remain unaffected. Our results further indicate that two additional residues in the AQP arginine filter may be involved in substrate selectivity: replacing one of the residues has a profound effect on water permeability, and replacing the other has a profound effect on Si permeability. This study has thus led to the identification of residues that could play a key role in Si transport by the AQGPs and shown that substrate selectivity is likely ensured by more than one checkpoint within or near the pore.

The Journal of General Physiology

INTRODUCTION

In mammals, the aquaporin (AQP) family is comprised of 13 isoforms that can be separated into three groups based on their permeability characteristics. One group includes AQP0, 1, 2, 4, 5, 6, and 8 (the conventional AQPs) that operate mainly as channels for water and accessorily as channels for cations (AQP1), urea (AQP6 and 8), nitrate (AQP6), and Cl (AQP6). Another group includes AQP3, 7, 9, and 10 (the aquaglyceroporins [AQGPs]) that also operate as channels for water but that exhibit selectivity for substrates such as polyols, H_2O_2, carbamides, monocarboxylates, nitrogenous bases, and metalloids. The last group includes AQP11 and 12 (the super AQPs) for which no defined transport functions have been identified yet (Rojek et al., 2008; Ishibashi et al., 2009).

Low silicone rice 1 (lsi1) is a transporter that also belongs to the AQP family and that can act as a permeation pathway for Si in the root's exodermis to allow transfer of this substrate from soil to phloem (Ma et al., 2006). Based on this finding, we recently tested the hypothesis that the human AQPs could also act as Si transporters even though they shared low amino acid identity with the plant protein. Interestingly, three members within the AQGP subgroup were found to play such a role given that their expression in *Xenopus laevis* oocytes induced robust and saturable Si transport activity (Garneau et al., 2015). The importance of these studies stemmed from the identification of Si transport systems in animals for the first time, of further evidence that Si is likely to support key biological functions, especially in connective tissues (Jugdaohsingh et al., 2008; Garneau et al., 2015), and of new opportunities to decipher the mechanisms of AQP-mediated substrate movement based on structure–function investigations.

AQPs are present in cell membranes as homotetramers. Within this structure, each of the monomers is formed of six transmembrane helices that are flanked by short intracellular termini (Fig. 1, A and B). High-resolution imaging of AQP1 in erythrocytes and of the AQP-like glycerol facilitator (GlpF) in *Escherichia coli* has revealed two regions of importance in the pore for determining selectivity and preventing water molecules from interacting with each other through hydrogen bonding. One region, the arginine filter (XX/R), is constituted of two noncontiguous residues (F-H in AQP1 and G-G in G1pF) that

Correspondence to Paul Isenring: paul.isenring@crhdq.ulaval.ca

Abbreviations used: Ab, antibody; AQGP, aquaglyceroporin; AQP, aquaporin.

The Rockefeller University Press $30.00
J. Gen. Physiol. 2016 Vol. 148 No. 3 239–251
www.jgp.org/cgi/doi/10.1085/jgp.201611598

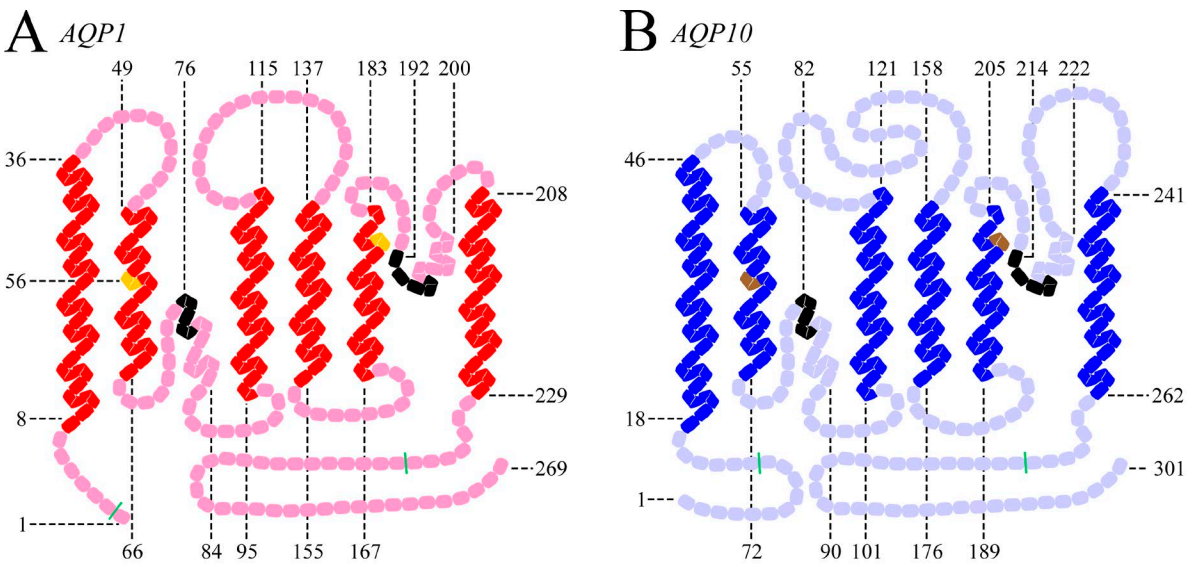

C

```
AQP0  MWELRSASFWRAIFAEFFATLFYVFFGLGSSLRWAPG-------PLHVLQVAMAFGLALATLVQSVGHISGAHVNPAVTFAFLVGSQM  081
AQP1  ASEFKKKLFWRAVVAEFLATTLFVFISIGSALGFKYPVGNNQTAVQDNVKVSLAFGLSIATLAQSVGHISGAHINPAVTLGLLLSCQI  089
AQP2  MWELRSIAFSRAVFAEFLATLLFVFFGLGSALNWPQA-------LPSVLQIAMAFGLGIGTLVQALGHISGAHINPAVTVACLVGCHV  081
AQP3  EMLHIRYRLLRQALAECLGTLILVMFGCGSVAQVVLS----RGTHGGFLTINLAFGFAVTLGILIAGQVSGAHLNPAVTFAMCFLARE  096
AQP4  FKGVWTQAFWKAVTAEFLAMLIFVLLSLGSTINWGGT---EKPLPVDMVLISLCFGLSIATMVQCFGHISGGHINPAVTVAMVCTRKI  110
AQP5  KKEVCSVAFLKAVFAEFLATLIFVFFGLGSALKWPSA-------LPTILQIALAFGLAIGTLAQALGPVSGGHINPAITLALLVGNQI  082
AQP6  LACRLWKAISRALFAEFLATGLYVFFGVGSVMRWPTA-------LPSVLQIAITFNLVTAMAVQVTWKASGAHANPAVTLAFLVGSHI  095
AQP7  IQEILQRKMVREFLAEFMSTYVMMVFGLGSVAHMVLN----K-KYGSYLGVNLGFGFGVTMGVHVAGRISGAHMNAAVTFANCALGRV  107
AQP8  WRVSWYERFVQPCLVELLGSALFIFIGCLSVIENGTD--------TGLLQPALAHGLALGLVIATLGNISGGHFNPAVSLAAMLIGGL  105
AQP9  QRLVLKSSLAKETLSEFLGTFILIVLGCGCVAQAILS----RGRFGGVITINVGFSMAVAMAIYVAGGVSGGHINPAVSLAMCLFGRM  097
AQP10 GHLRIRSLLARQCLAEFLGVFVLMLLTQGAVAQAVTS----GETKGNFFTMFLAGSLAVTIAIYVGGNVSGAHLNPAFSLAMCIVGRL  096

AQP0  SLLRAFCYMAAQLLGAVAGAAVLYSVTPPAVRGN---------------LALNTLHPAVSVGQATTVEIFLTLQFVL--CIFATYDER  152
AQP1  SIFRALMYIIAQCVGAIVATAILSGITSSLTGNS---------------LGRNDLADGVNSGQGLGIEIIGTLQLVL--CVLATTDRR  160
AQP2  SVLRAAFYVAAQLLGAVAGAALLHEITPADIRGD---------------LAVNALSNSTTAGQAVTVELFLTLQLVL--CIFASTDER  152
AQP3  PWIKLPIYTLAQTLGAFLGAGIVFGLYYDAIWHFADNQLFVSGPNGTAGIFATYPSGHLDMINGFFDQFIGTASLIV--CVLAIVDPY  182
AQP4  SIAKSVFYIAAQCLGAIIGAGILYLVTPPSVVGG---------------LGVTMVHGNLTAGHGLLVELIITFQLVF--TIFASCDSK  181
AQP5  SLLRAFFYVAAQLVGAIAGAGILYGVAPLNARGN---------------LAVNALNNNTTQGQAMVVELILTFQLAL--CIFASTDSR  153
AQP6  SLPRAVAYVAAQLVGATVGAALLYGVMPGDIRET---------------LGINVVRNSVSTGQAVAVELLLTLQLVL--CVFASTDSR  166
AQP7  PWRKFPVYVLGQFLGSFLAAATIYSLFYTAILHFSGGQLMVTGPVATAGIFATYLPDHMTLWRGFLNEAWLTGMLQL--CLFAITDQE  193
AQP8  NLVMLLPYWVSQLLGGMLGAALAKAVSPEERFWN------------ASGAAFVTVQEQGQVAGALVAEIILTTLLALAVCMGAINEKT  181
AQP9  KWFKLPFYVGAQFLGAFVGAATVFGIYYDGLMSFAGGKLLIVGENATAHIFATYPAPYLSLANAFADQVVATMILLI--IVFAIFDSR  183
AQP10 PWVKLPIYILVQLLSAFCASGATYVLYHDALQNYTGGNLTVTGPKETASIFATYPAPYLSLNNGFLDQVLGTGMLIV--GLLAILDRN  181

AQP0  RNG-QLGSVALAVGFSLALGHLFGMYYTGAGMNPARSFAPAILTG-----------NFTNHWVYWVGPIIGGGLGSLLYDFLLFPRLK  228
AQP1  RRD-LGGSAPLAIGLSVALGHLLAIDYTGCGINPARSFGSAVITH-----------NFSNHWIFWVGPFIGGALAVLIYDFILAPRSS  236
AQP2  RGE-NPGTPALSIGFSVALGHLLGIHYTGCSMNPARSLAPAVVTG-----------KFDDHWVFWIGPLVGAILGSLLYNYVLFPPAK  228
AQP3  NNPVPRGLEAFTVGLVVLVIGTSMGFNSGYAVNPARDFGPRLFTALAGWGSAVFTTGQHWWWVPIVSPLLGSIAGVFVYQLMIGCHLE  270
AQP4  RTD-VTGSIALAIGFSVAIGHLFAINYTGASMNPARSFGPAVIMG-----------NWENHWIYWVGPIIGAVLAGGLYEYVFCPDVE  257
AQP5  RTS-PVGSPALSIGLSVTLGHLVGIYFTGCSMNPARSFGPAVVMN----------RFSPAHWVFWVGPIVGAVLAAILYFYLLFPNSL  230
AQP6  QT---SGSPATMIGISVALGHLIGIHFTGCSMNPARSFGPAIIIG-----------KFTVHWVFWVGPLMGALLASLIYNFVLFPDTK  240
AQP7  NNPALPGTEALVIGILVVIIGVSLGMNTGYAINPSRDLPPRIFTFIAGWGKQVFSNGENWWWVPVVAPLLGAYLGGIIYLVFIGSTIP  281
AQP8  ----KGPLAPFSIGFAVTVDILAGGPVSGGCMNPARAFGPAVVAN-----------HWNFHWIYWLGPLLAGLLVGLLIRCFIGDGKT  254
AQP9  NLGAPRGLEPIAIGLLIIVIASSLGLNSGCAMNPARDLSPRLFTALAGWGFEVFRAGNNFWWIPVVGPLVGAVIGGLIYVLVIEIHHP  271
AQP10 NKGVPAGLEPVVVGMLILALGLSMGANCGIPLNPARDLGPRLFTYVAGWGPEVFSAGNGWWWVPVVAPLVGATVGTATYQLLVALHHP  269
```

Figure 1. **Hydropathy plot models and transport characteristics of wild-type AQP1 and AQP10.** (A) Model of AQP1. Each symbol corresponds to a single residue within a transmembrane domain (red), a connecting segment (pink), the XX/R filter (yellow), or the NPA motifs (black). Residues above the transmembrane domains face the extracellular side of the membrane. The cartoon was drawn with the program PLOT based on the hydropathy model of Murata et al. (2000). (B) Model of AQP10. Each symbol corresponds to a single residue in a transmembrane domain (blue), a connecting segment (pale blue), the XX/R filter (brown), or the NPA motifs (black). The cartoon was drawn with the program PLOT based on sequence alignments of transmembrane domains with AQP1. (C) Multiple alignment analysis of AQP family members with Clustal Omega. The residue segment used for each of the channels corresponds to the one that is flanked by green lines in A and B; the N and C termini were excluded from the analysis given that they are poorly conserved among the isoforms. AQP11 and AQP12 were also excluded given that they share much lower homologies with the other family members. Gray boxes correspond to transmembrane segments based on alignments with AQP1, and colored residues correspond to those that were interchanged between AQP1 and AQP10 in this study.

lies next to a highly conserved arginine residue. In AQP1, it constricts the pore to a minimal diameter of ~2.8 Å and in G1pF to a minimal diameter of ~3.4 Å. The other region of importance is very close to the constriction site and is constituted of two NPA motifs that are each provided by a connecting loop and that probably operate as dipoles to reorient water molecules during their passage through the channel (Braun et al., 2000; Murata et al., 2000; Ren et al., 2000; Wang et al., 2005).

The mechanisms invoked to explain how the pore of AQPs achieves selectivity are not perfectly satisfying. In particular, size constraint imposed by the XX/R filter has been said to play a crucial role (Ishibashi et al., 1997; Holm et al., 2005; Herrera et al., 2006; Bienert et al., 2007; Hachez and Chaumont, 2010). Yet, a variety of substrates are able to permeate the conventional AQPs even though their effective, hydrated atomic diameter (>3.0 Å for Na and Cl) exceeds that predicted for the region of maximal constriction. Likewise, several substrates are virtually unable to permeate the AQGPs even though their atomic diameter (<3 Å for water and nitrate) should allow them to do so based on size. It has also been suggested that the pair of NPA motifs were key in allowing water movement through the pore. As can be seen in the alignments of Fig. 1, however, these motifs are present in most of the AQPs, whereas permeability to water varies substantially among the isoforms (Ishibashi et al., 2009).

The identification of novel transport functions for the AQP represents an opportunity to further our understanding of solute permeation through the pore. In particular, several residues localized near or at the region of channel constriction differ between conventional AQPs and AQGPs while being conserved among the AQGPs. The residue stretch flanked by the NPA motifs is also less conserved between the two groups of AQPs than it is among members within each group of water channels (see alignments of Fig. 1 once again).

In this study, selectivity-modifying residues were identified by examining the effect of interchanging nonconserved residues between AQP1 and AQP10, i.e., between channels that exhibit opposite behaviors in regard to both Si and water transport. Two such residues were part of the XX/R filter, one was in the second transmembrane domain before the first NPA motif, five were in the second extracellular loop, and one was in the third extracellular loop before the second NPA motif (Fig. 1). Our results suggest that a specific combination of residues within the XX/R filter is necessary for the AQPs to play the role of Si channel but not to play that of a water channel. Our results also led to the identification of two selectivity-specifying residues outside of the XX/R filter, one that may be key in facilitating water permeation and another one that may be key in facilitating Si permeation.

MATERIALS AND METHODS

Supplies

Reagents or kits included the QuikChange site-directed mutagenesis kit and XL1-blue competent cells (Agilent Technologies); various enzymes and buffers for DNA construction (New England Biolabs, Inc.); a horseradish peroxidase–conjugated sheep anti–mouse anti-IgG, a horseradish peroxidase–conjugated donkey anti–rabbit anti-IgG, and the ECL Western Blotting Detection Reagents kit (GE Healthcare); EZ-link sulfo-NHS-Biotin, various salts, reagents and buffers for media preparation, a rabbit anti-AQP10 antibody (Ab), and oligonucleotides (Sigma-Aldrich); the Rapid DNA ligation kit and protease inhibitors (Roche); the T7 mMESSAGE mMACHINE kit and Dynabeads MyOne Streptavidin T1 (Invitrogen); the anti–rabbit Alexa Fluor 488–conjugated Ab and the anti–mouse Alexa Fluor 594–conjugated Ab (Molecular Probes); and Tissue-Tek O.C.T. compound (VWR) and a mouse anti-AQP1 monoclonal Ab (Abcam).

Point mutations

Point mutations were already available from previous work, AQP1 and AQP10 cloned in an oocyte expression vector (PolI) that contains the following sequences (from 5′ to 3′): the T7 bacterial promoter, the 5′ untranslated region of the *Xenopus* β-globin gene, a multiple cloning site, the 3′ untranslated region of the *Xenopus* β-globin gene, a poly A tract, and a linearizing site (Garneau et al., 2015). These constructs were used as template to produce 12 mutants that are listed in Table 1 along with the oligonucleotide primers exploited. The localization of the residues substituted is also shown in Fig. 2 (C and D).

Chimeras

Two different chimeras were generated from AQP1 and AQP10. The first one, $AQP_{1\text{-}10\text{-}1}$, consisted of AQP1 in which the segment enclosed between the NPA sites (residues 79–191) was substituted by that of AQP10 (residues 85–215), whereas the second one, $AQP_{10\text{-}1\text{-}10}$, consisted of the reciprocal chimera. These mutants, which are illustrated in Fig. 2 (A and B), were created by fragment exchange after introducing a PmlI restriction site before the first NPA motif and a SacII restriction site after the second NPA motif in both AQP1 and AQP10 (oligonucleotides used are listed in Table 1).

Channel expression

In all experiments, stage-V oocytes were injected with ~15 ng cRNA in 50 nl water or with 50 nl water alone to obtain background data. After injection, oocytes were maintained at 18°C for 72 h in medium B1 (see media composition in Table 2) to allow channel synthesis, and

Table 1. **Mutants generated and oligonucleotides used**

Name	Mutagenic oligonucleotides
$AQP1_{L84C}$	5′ gtcacactggggctgTGCctTagctgccagatcag
	3′ ctgatctggcagctAagGCAcagccccagtgtgac
$AQP1_{H180G}$	5′ ctctctgtagcccttggaGGCctcctggctattgacAAC
	3′ GTTgtcaatagccaggagGCCtccaagggctacagagag
$AQP1_{F56G/H180G}$	5′ gaaggtgtcgctggccGGCgggctgagcatcg
	3′ cgatgctcagcccGCCggccagcgacaccttc
$AQP1_{Y186N}$	5′ ggaggCctcctggcAattgacAACactggctgtggg
	3′ cccacagccagtGTTgtcaatTgccaggagGcctcc
$AQP1_{LGRND\leftrightarrow IFATY}$	5′ ctgactgggaactcgATTTTTGCCACCTATctggctgatggtgtg
	3′ cacaccatcagccagATAGGTGGCAAAAATcgagttcccagtcag
$AQP10_{C90L}$	5′ ccttctccctggccatgCTCatcgttggacgcctccc
	3′ gggaggcgtccaacgatGAGcatggccagggagaagg
$AQP10_{G202H}$	5′ ctgatcctggccctcCACttatcTatgggtgcc
	3′ ggcacccatAgataaGTGgagggccaggatcag
$AQP10_{G62F/G202H}$	5′ gtttctggctTTctctctggccgttacgatCgccatctacgtg
	3′ cacgtagatggcGatcgtaacggccagagagAAagccagaaac
$AQP10_{N208Y}$	5′ ggccctcgggttatcTatgggtgccTACtgcgggattccactc
	3′ gagtggaatcccgcaGTAggcacccatAgataacccgagggcc
$AQP10_{IFATY\leftrightarrow LGRND}$	5′ aaggagacagcctccCTTGGCCGCAATGACcctgccccctatctg
	3′ cagataggggcaggGTCATTGCGGCCAAGggaggctgtctcctt
+PmlI in AQP1	5′ atcagcggcgcccacgtgAACCCGGCTgtcac
	3′ gtgacAGCCGGGTTcacgtgggcgccgctgat
+SacII in AQP1	5′ tgtgggattAACCCTCCGcggtcctttggctcc
	3′ ggagccaaaggaccgCGGAGGGTTaatcccaca
+Pml1 in AQP10	5′ gtctcaggggcccacgtgAATCCAGCCttc
	3′ gaaGGCTGGATTcacgtgggcccctgagac
+SacII in AQP10	5′ gtctcaggggcccacgtgAATCCAGCCttc
	3′ tgggcccaggtcccgCGGAGGGTTgagtggaat
5′ $AQP_{1\text{-}10\text{-}1}$	5′ atcagcggcgcccacctcAATCCAGCCttctcc
	3′ ggagaaGGCTGGATTgaggtgggcgccgctgat
3′ $AQP_{1\text{-}10\text{-}1}$	5′ attccactcAACCCTGCCcggtcctttggctcc
	3′ ggagccaaaggaccgGGCAGGGTTgagtggaat
5′ $AQP_{10\text{-}1\text{-}10}$	5′ gtctcaggggcccacctgAACCCGGCTgtcac
	3′ gtgacAGCCGGGTTcaggtgggcccctgagac
3′ $AQP_{10\text{-}1\text{-}10}$	5′ tgtgggattAACCCTGCTcgggacctgggccca
	3′ tgggcccaggtcccgAGCAGGGTTaatcccaca

Uppercase letters correspond to a base pair that was mutated to generate a residue substitution, to remove a restriction site or to add a restriction site.

after this interval, they were used for different experiments as detailed in the next four sections.

Water transport

Water permeability was determined as previously described after incubating oocytes in plain water for 180 s (Beitz et al., 2006). During this period of time, cells were photographed every 6 s under brightfield microscopy, and the images acquired were analyzed with the NIS-Elements 3.0 software to measure cross sections (A). From the A values obtained, oocyte volumes (V) were calculated as $V = (4/3) \times A \times (A/\pi)^{1/2}$, and from the V values obtained, permeability coefficients (*Pf*) were calculated as $Pf = [V_0 \times d(V/V_0)/dt]/[S \times V_w \times (osm_i - osm_o)]$, where V_0 = initial volume (9×10^{-4} cm^3), $d(V/V_0)/dt$ = oocyte swelling rate, S = initial surface (0.045 cm^2), V_w = molar volume of water (18 cm^3/mol), osm_i = intracellular osmolality (200 mOsM), and osm_o = extracellular osmolality (0 mOsM).

Si influx

Oocytes were placed in medium B2 for 90 min, a time scale during which Si transport by AQP10 is linear as a function of time. After several rinses in 10 mM Na HEPES and 180 mM sucrose, oocytes (10 per assay) were dissolved in 70% nitric acid, the resulting sample was dehydrated on a warming plate, the pellet formed was suspended in 1 ml ultrapure water, and the final mixture was assayed for Si content through atomic absorption spectrophotometry using the AA240Z Zeeman atomic spectrometer with its GTA120 graphite tube.

Expression experiments

Oocytes (75–80 per assay) were placed in medium B3 (see composition in Table 2) added with 2 mM sulfo-NHS biotin for 45 min to label cell surface proteins exclusively. After several washes in medium B3 added with 10 mM glycine, oocytes were lysed in 20 mM Tris, pH 8.0,

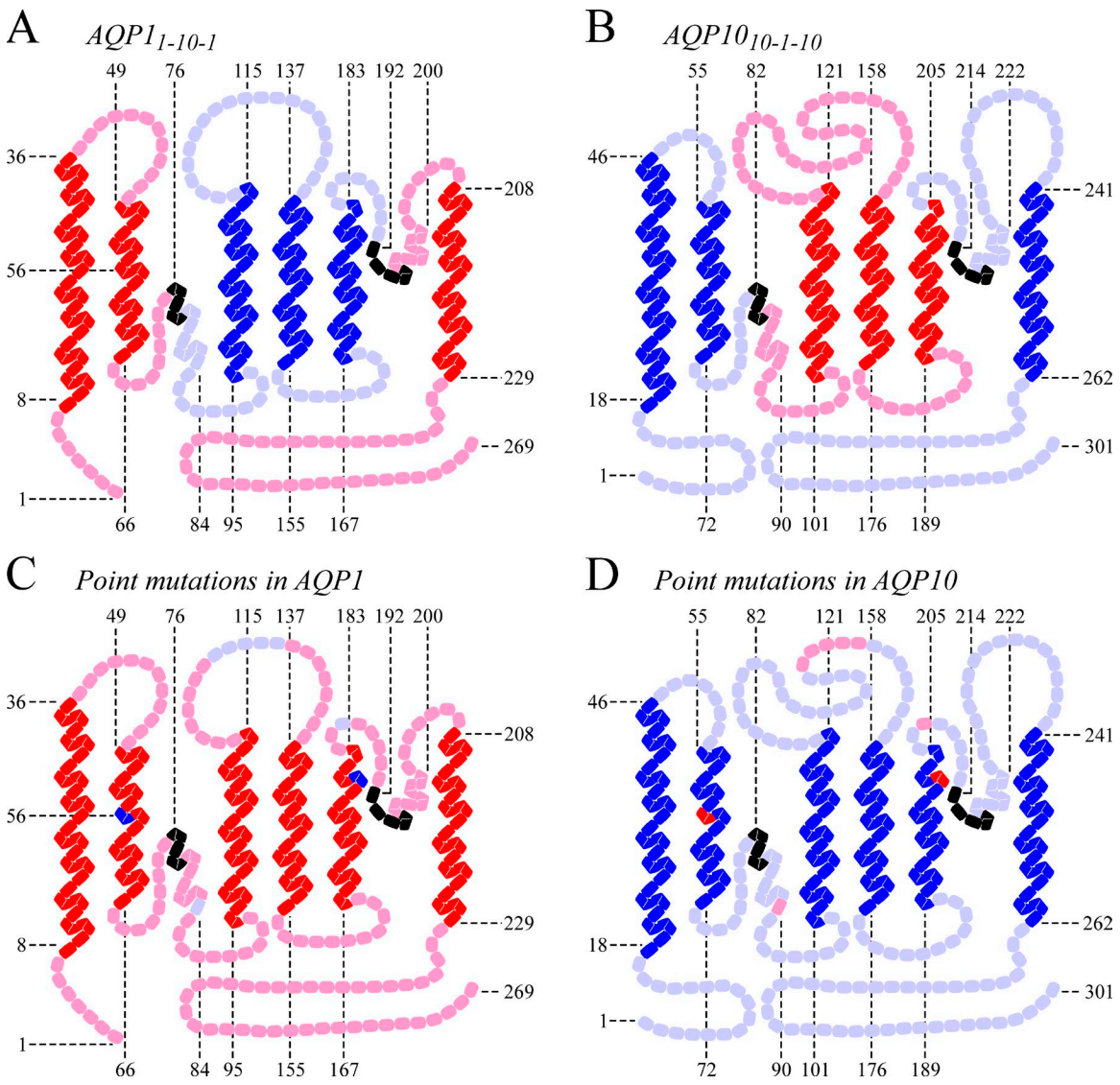

Figure 2. **Location of residues that were substituted in AQP1 and AQP10.** The cartons were drawn as described in Fig. 1 using the same color code. (A and B) Chimeras. (C and D) Point substitutions.

1 mM EDTA, 4 mM $MgCl_2$, 10% glycerin, 1% Triton-X, and a cocktail of protease inhibitors, homogenates obtained were mixed with 50 µl of streptavidin-coupled Dynabeads, bead-bound cell surface proteins were purified through repeated wash cycles, bead-bound cell surface AQPs were detected through chemiluminescence-based Western blot analyses, and CCC-specific signals were quantified by band densitometry.

Immunofluorescence

Experiments were performed as described previously (Gagnon et al., 2004, 2005; Bergeron et al., 2006). In brief, 10-µm oocyte cryosections were postfixed in 4% paraformaldehyde for 30 min, after which they were incubated sequentially with a primary monoclonal Ab for 16 h at 4°C and with a secondary Ab for 1 h at room temperature. AQP-specific signals

Table 2. **Composition of media**

Media	Na^+	K^+	Cl^-	Ca^{2+}	Mg^{2+}	SO_4^{2-}	NO_3^-	HCO_3^-	Si	HEP	NMG	GLU	pH	OsM
B1	96	1.0	85	0.8	0.8	0.8	0.7	2.5	0.0	10.0	1.0	1.0	7.4	200
B2	96	1.0	85	0.8	0.8	0.8	0.7	2.5	2.0	10.0	0.0	0.0	7.4	200
B3	88	7.0	89	2.0	2.0	1.0	0.0	0.0	0.0	10.0	0.0	0.0	7.4	200

Abbreviations are HEP = HEPES, NMG = *N*-methyl-D-glucamine, GLU = gluconate, OsM = osmolality. Except for pH and OsM, all units are in mM.

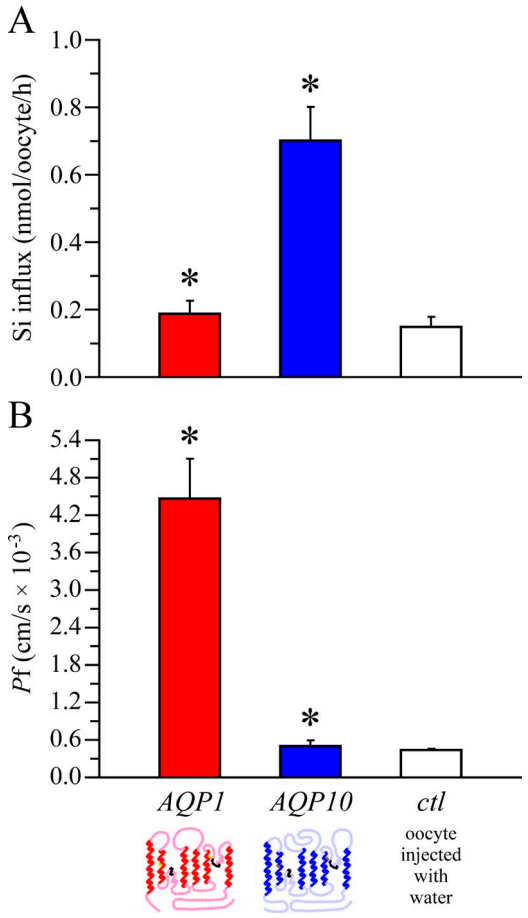

Figure 3. **Si influx in oocytes expressing AQP1, expressing AQP10, or injected with water.** (A) Oocytes incubated in medium B2 for 90 min at room temperature were assayed for Si content. Data are expressed as means ± SE of 10 oocytes among 25–26 experiments, using the asterisk to indicate that they are significantly different statistically (*, $P < 0.05$) compared with oocytes injected with water. (B) Water permeability in oocytes expressing AQP1, expressing AQP10, or injected with water. Oocytes incubated in plain water were assayed for volume measurements as described in Materials and methods. Data are expressed as mean *Pf* ± SE of three to five oocytes among five to six experiments, using the asterisk to indicate that they are significantly different statistically (*, $P < 0.05$) compared with oocytes injected with water.

were subsequently photographed under confocal microscopy at 60×.

Sequence and statistical analyses

All of the wild-type and mutant cDNAs produced were characterized by restriction analyses and automated sequencing using vector- or insert-specific primers. Protein alignment between AQP1 and AQP10 was generated after pairing each of the transmembrane segments between the isoforms. Data obtained (absolute or normalized) are presented as means of concurrent determinations ± SE. Differences between datasets were analyzed by Welch's *t* tests and considered statistically significant at $P < 0.05$.

RESULTS

Wild-type AQPs

The transport characteristics of AQP1 and AQP10 are summarized in Fig. 3. They are from determinations that were obtained for this study specifically. As shown in Fig. 3 A, Si transport by oocytes expressing AQP1 is very low (1.3-fold above background), whereas Si transport by oocytes expressing AQP10 is much higher (4.7-fold above background). As shown in Fig. 3 B, in contrast, water transport in oocytes expressing AQP1 is substantial (10.2-fold above background), whereas water transport in oocytes expressing AQP10 is much lower (1.1-fold above background).

These results are consistent with those reported by our group (Garneau et al., 2015) in a recent publication on the identification of novel Si transporters in humans. Additionally, they confirm that the AQPs chosen for the current analysis can serve as relevant models to identify selectivity-modifying residues. Indeed, one acts as a robust water channel but inefficient Si transporter, whereas the other exhibits mirror-image characteristics in this regard.

Data presentation for the mutants

In Figs. 4, 5, 6, 7, and 8, Si and water transport data are expressed as *n*-fold differences between a specific mutant and its wild-type counterpart after background subtraction and normalization to the amount of channels expressed at the cell surface. By way of illustration, this difference (F) for an AQP mutant was calculated as follows: $F = [(I_{Si}\ \text{mutant} - I_{Si}\ \text{ctl})/(I_{Si}\ \text{wt} - I_{Si}\ \text{ctl})/(EXP\ \text{mutant} - EXP\ \text{wt})]$, where I_{Si} = Si transport rate, mutant = oocytes expressing the mutant AQP, ctl = oocytes injected with water, wt = oocytes expressing the wild-type AQP, and *EXP* = expression level at the cell surface. Based on this approach, it is expected that if an AQP1 mutant induces no gain of function in Si influx, the *n*-fold difference between this mutant and wild-type AQP1 will be equal to 1 given that oocytes expressing AQP1 do not exhibit above-background Si transport. Likewise, it is expected that if an AQP10 mutant induces no gain of function in water transport, the *n*-fold difference between this mutant and wild-type AQP10 will also be equal to 1 given that oocytes expressing AQP10 do not exhibit above-background water transport. Note that the primary data used for the calculations are also listed in Table 3 and that channel expression was not used to normalize the transport data of either chimera given that it was greatly reduced.

Chimeras

The entire residue stretch that begins with the first NPA motif and ends with the second one was interchanged between the two isoforms to generate the

Table 3. **Absolute Si influx and *Pf* values for wild-type and mutant channels**

Channels	Si influx	Water permeability	Expression
	nmol/oocyte/h	*cm/s × 10^{-3}*	*relative units*
AQP1	0.39 ± 0.08	4.027 ± 0.578	1.00 ± 0.00
$AQP1_{LGNRD\leftrightarrow IFATY}$	0.37 ± 0.06	0.214 ± 0.148[a]	0.90 ± 0.27[a]
$AQP1_{L84C}$	0.37 ± 0.09	0.957 ± 0.333[a]	0.91 ± 0.20[a]
$AQP1_{Y186N}$	2.60 ± 0.59[a]	3.624 ± 0.149	0.92 ± 0.04[a]
$AQP1_{F56G/H180G}$	2.17 ± 0.36[a]	3.844 ± 0.800	0.94 ± 0.03
AQP10	5.53 ± 0.79	0.060 ± 0.012	1.00 ± 0.00
$AQP10_{IFATY\leftrightarrow LGNRD}$	0.63 ± 0.28[b]	0.071 ± 0.001	0.99 ± 0.07
$AQP10_{C90L}$	5.43 ± 1.79	0.254 ± 0.028[b]	0.93 ± 0.06[b]
$AQP10_{N208Y}$	2.13 ± 0.71[b]	0.076 ± 0.003	1.10 ± 0.26
$AQP10_{G62F/G202H}$	2.27 ± 0.43[b]	0.090 ± 0.021	1.39 ± 0.21[b]

Values shown correspond to background-subtracted data, that is, data obtained in AQP-expressing oocytes − data obtained in water-injected oocytes. In the expression experiments, background-subtracted data were divided further by the quantity of channels present at the surface of AQP1- or AQP10-expressing oocytes. For all of the mutants, data are expressed as means ± SE of 3–10 oocytes among three to six experiments.
[a]Data are significantly different statistically ($P < 0.05$) compared with AQP1-expressing oocytes.
[b]Data are significantly different statistically ($P < 0.05$) compared with AQP10-expressing oocytes.

chimeras $AQP_{1\text{-}10\text{-}1}$ and $AQP_{10\text{-}1\text{-}10}$ (illustrated in Fig. 2 [A and B]). The transport characteristics and cell surface expression levels of both these mutants are shown in Fig. 4.

It is seen that Si influx in oocytes expressing $AQP_{10\text{-}1\text{-}10}$ is considerably lower than in oocytes expressing AQP10 (Fig. 4 A) and that water transport in oocytes expressing $AQP_{1\text{-}10\text{-}1}$ is considerably lower than in oocytes expressing AQP1 (Fig. 4 B). It is also seen that both chimeras are poorly expressed at the cell surface relative to the wild-type channels (Fig. 4 C). Given that their expression was very low in whole cell lysates as well (not depicted), these results indicate that the mutations prevented the channels from being synthesized normally or led them to be abnormally sensitive to post-translational degradation.

$AQP_{LGRND\leftrightarrow IFATY}$

In the middle extracellular loop of conventional AQPs and AQGPs at an equidistant distance between the NPA motifs, a stretch of five contiguous residues (124–128 in AQP1 and 145–149 in AQP10) was found to be highly conserved within each group of channels but poorly conserved between the two groups. It was thus interchanged in each channel with that of the other and the resulting mutants, $AQP1_{LGRND\rightarrow IFATY}$ and $AQP10_{IFATY\rightarrow LGRND}$ (illustrated in Fig. 2 [C and D]), were analyzed as described for the chimeras.

Results, which are shown in Fig. 5, reveal that the transport characteristics of oocytes expressing $AQP1_{LGRND\rightarrow IFATY}$ are similar to oocytes expressing $AQP1_{1\text{-}10\text{-}1}$ and those of oocytes expressing $AQP10_{IFATY\rightarrow LGRND}$ similar to oocytes expressing $AQP10_{10\text{-}1\text{-}10}$ (Fig. 5, A and B). How-

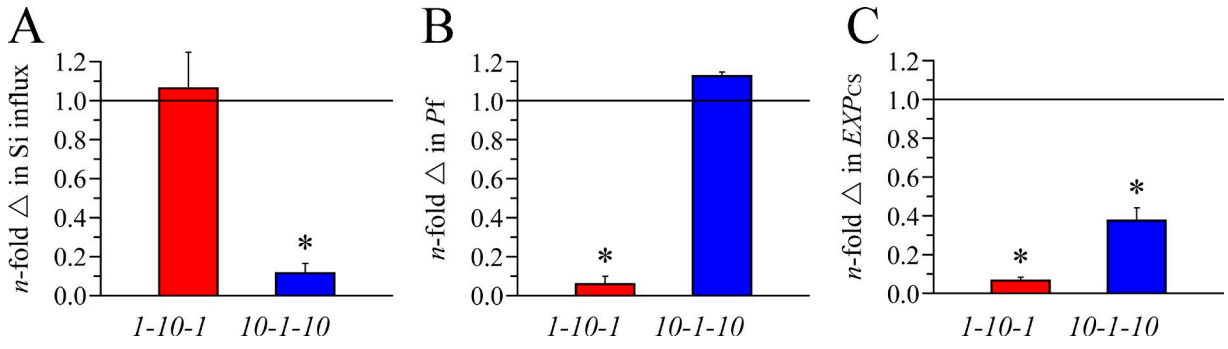

Figure 4. **Transport characteristics and membrane expression of $AQP1_{1\text{-}10\text{-}1}$ and $AQP10_{10\text{-}1\text{-}10}$.** (A) Si influx. Oocytes incubated in medium B2 for 90 min at room temperature were assayed for Si content. They were from 10 oocytes among three to four experiments. According to this presentation, a mean of 1 indicates no *n*-fold differences (Δ) in Si influx. (B) Water permeability. Oocytes incubated in plain water were assayed for volume measurements as described in Materials and methods. They were from three to five oocytes among three experiments. (A and B) Data are expressed as *n*-fold differences ± SE between $AQP1_{1\text{-}10\text{-}1}$ and AQP1 (left bar) or between $AQP10_{10\text{-}1\text{-}10}$ and AQP10 (right bar) after background subtraction and normalization to channel expression levels. (C) AQP expression at the cell surface (*EXPcs*). Oocytes incubated in medium B2 for 90 min were lysed for Western blot analyses using specific anti-AQP Abs, and the signals obtained were quantified through densitometry. Data are expressed as *n*-fold differences ± SE between $AQP1_{1\text{-}10\text{-}1}$ and AQP1 (left bar) or between $AQP10_{10\text{-}1\text{-}10}$ and AQP10 (right bar) after background subtraction. They were from three experiments. (A–C) The asterisk is used to indicate that the mean is significantly different statistically (*, $P < 0.05$) compared with the wild-type channel.

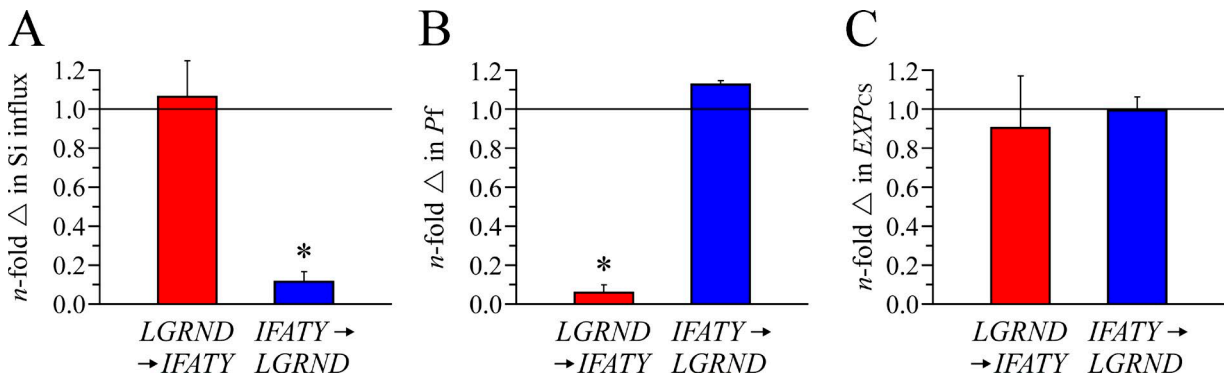

Figure 5. **Transport characteristics and membrane expression of AQP1$_{LGRND→IFATY}$ and AQP10$_{IFATY→LGRND}$.** Experimental conditions were as described in Fig. 4. Data expression is also as described in Fig. 4. (A) Si influx. Data are expressed as means ± SE of 10 oocytes among three experiments. (B) Water permeability. Data are expressed as means ± SE of three to five oocytes among three to four experiments. (A and B) The asterisk is used to indicate that the mean is significantly different statistically (*, $P < 0.05$) compared with the wild-type channel. (C) AQP expression at the cell surface (*EXPcs*). Data are expressed as means ± SE among three to four experiments.

ever, the LGRND↔IFATY substitutions are not seen to affect cell surface expression substantially compared with the wild-type channels (Fig. 5 C), indicating that they could have simply resulted in steric occlusion of the pore through conformational changes. It is of notice in this regard that the residue stretch in AQP10 is comprised of four hydrophobic amino acids, whereas that in AQP1 is comprised of only one.

AQP1$_{L84C}$ and AQP10$_{C90L}$

Residue 84 in AQP1 and 90 in AQP10 are also highly conserved within each group of channels but poorly conserved between the two groups. It is slightly downstream of the proximal NPA motif, but at some distance from the XX/R filter (see Discussion). The effect of interchanging these residues to produce AQP1$_{L84C}$ and AQP10$_{C90L}$ (illustrated in Fig. 2 [C and D]) is presented in Fig. 6.

As seen, Si influx between oocytes expressing AQP1$_{L84C}$ and oocytes expressing AQP1 is similar and so is Si influx between oocytes expressing AQP10$_{C90L}$ and oocytes expressing AQP10 (Fig. 6 A). In contrast, water permeability in oocytes expressing AQP1$_{L84C}$ is approximately fourfold lower than in oocytes expressing AQP1, and water permeability in oocytes expressing AQP10$_{C90L}$ is approximately fourfold higher than in oocytes expressing AQP10 (Fig. 6 B), whereas cell surface expression is the same for both mutants relative to their wild-type counterpart (Fig. 6 C). It is noteworthy that the fold difference in *Pf* between oocytes expressing AQP1$_{L84C}$ and oocytes expressing AQP10$_{C90L}$ is in fact quite high (~17 in Fig. 6 B).

Collectively, these results imply that residue L$_{84}$ in AQP1 might be key to transporting water molecules. They also indicate that in regard to water transport, the L84C substitution in AQP1 led to a loss of function and the C90L substitution in AQP10 led to a gain of function, i.e., to a pattern of effects that is consistent with reciprocal behaviors elicited through reciprocal mutations as is often the case when the residues exchanged

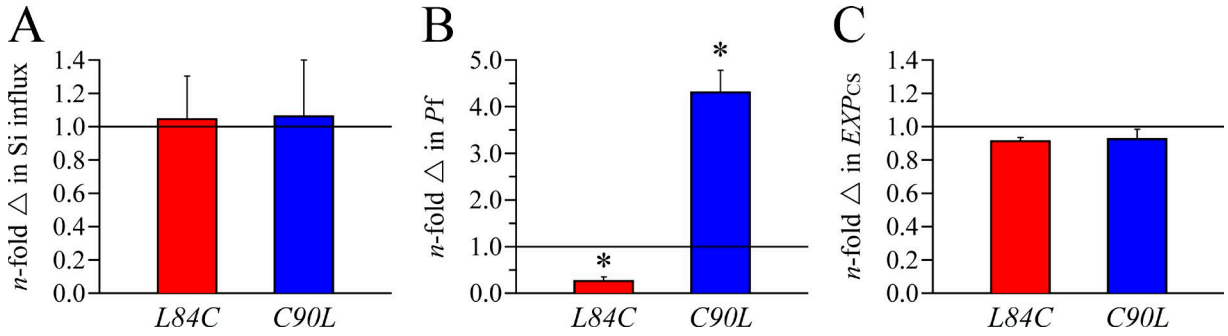

Figure 6. **Transport characteristics and membrane expression of AQP1$_{L84C}$ and AQP10$_{C90L}$.** Experimental conditions were as described in Fig. 4. Data expression is also as described in Fig. 4. (A) Si influx. Data are expressed as means ± SE of 10 oocytes among three to six experiments. (B) Water permeability. Data are expressed as means ± SE of three to five oocytes among three to four experiments. (B) The asterisk is used to indicate that the mean is significantly different statistically (*, $P < 0.05$) compared with the wild-type channel. (C) AQP expression at the cell surface (*EXPcs*). Data are expressed as means ± SE among three to four experiments.

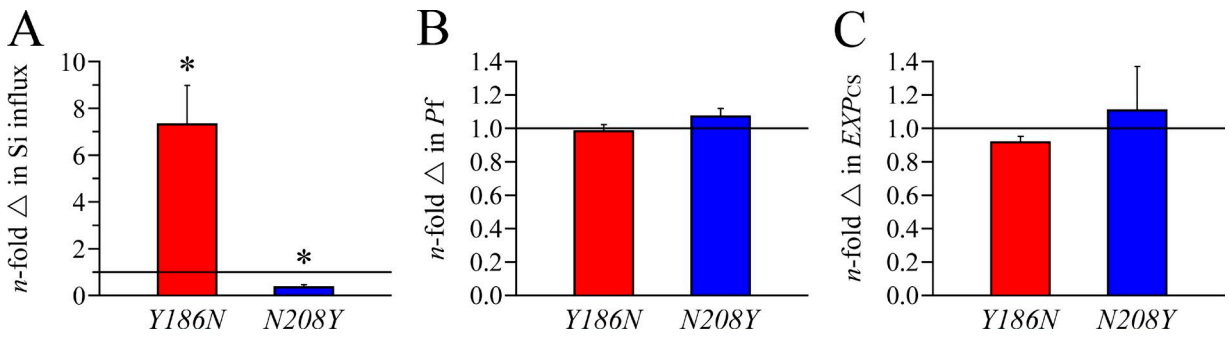

Figure 7. **Transport characteristics and membrane expression of AQP1$_{Y186N}$ and AQP10$_{N208Y}$.** Experimental conditions were as described in Fig. 4. Data expression is also as described in Fig. 4. (A) Si influx. Data are expressed as means ± SE of 10 oocytes among three to four experiments. The asterisk is used to indicate that the mean is significantly different statistically (*, $P < 0.05$) compared with the wild-type channel. (B) Water permeability. Data are expressed as means ± SE of three to five oocytes among three to four experiments. (C) AQP expression at the cell surface (*EXPcs*). Data are expressed as means ± SE among three experiments.

are functionally relevant (Gagnon et al., 2004, 2005; Deshmukh et al., 2015).

AQP1$_{Y186N}$ and AQP10$_{N208Y}$

Residue 186 in AQP1 is localized in an extracellular loop and also at some distance from the XX/R filter (see Discussion). It shares with residue 84 the same homology features among the AQP family. The transport and expression features of both mutants (illustrated in Fig. 2 [C and D]) are summarized in Fig. 7.

It is observed that Si influx by oocytes expressing AQP1$_{Y186N}$ is approximately sevenfold higher compared with oocytes expressing AQP1, whereas Si influx by oocytes expressing AQP10$_{G62F/G202H}$ is approximately threefold lower compared with oocytes expressing AQP10. Once again, the substitutions have led to reciprocal behaviors, but this time in regard to Si transport, and they indicate that residue N_{208} in AQP10 might be key to transporting Si. Noticeably, water transport for both mutants was similar compared with their wild-type counterparts.

AQP1$_{F56G/H180G}$ and AQP10$_{G62F/G202H}$

The last two mutants analyzed in this work were generated by interchanging two noncontiguous residues between AQP1 and AQP10. These residues are not only poorly conserved between the two groups of channels and highly conserved within each one, but they are also both constituents of the XX/R filter. Fig. 8 is used to present the transport properties and cell surface expression levels of AQP1$_{F56G/H180G}$ and AQP10$_{G62F/G202H}$ (illustrated in Fig. 2 [C and D]).

The data obtained are seen to be similar to those obtained for the AQP1$_{Y186N}$ and AQP10$_{N208Y}$ mutants. Indeed, Si influx by oocytes expressing AQP1$_{F56G/H180G}$ is approximately sixfold higher compared with oocytes expressing AQP1, Si influx by oocytes expressing AQP10$_{G62F/G202H}$ is approximately threefold lower compared with oocytes expressing AQP10 (Fig. 8 A), water transport is unaffected by the mutations (Fig. 8 B), and the same is true for cell surface expression (Fig. 8 C). Residues G_{62} and G_{202} in AQP10 might thus also be key to transporting Si. Note that when either of these two residues were re-

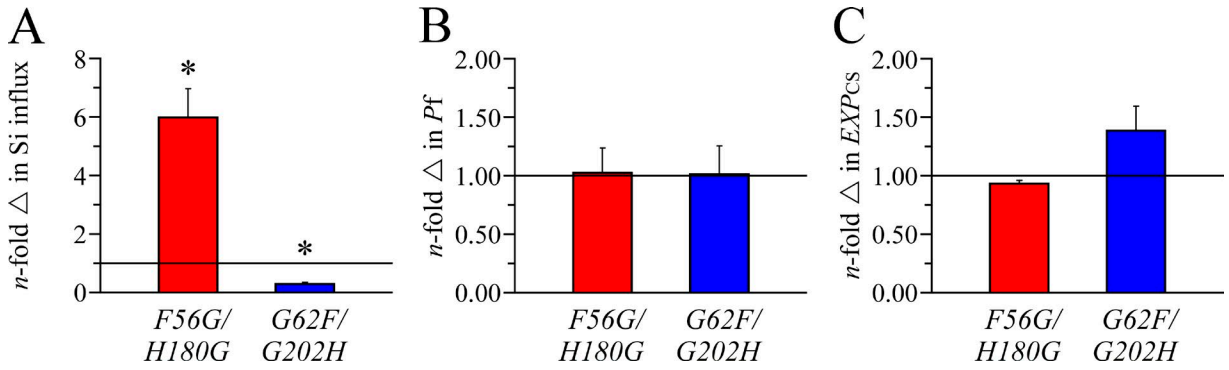

Figure 8. **Transport characteristics and membrane expression of AQP1$_{F56G/H180G}$ and AQP10$_{G62F/G202H}$.** Experimental conditions were as described in Fig. 4. Data expression is also as described in Fig. 4. (A) Si influx. Data are expressed as means ± SE of 10 oocytes among eight to nine experiments. The asterisk is used to indicate that the mean is significantly different statistically (*, $P < 0.05$) compared with the wild-type channel. (B) Water permeability. Data are expressed as means ± SE of three to five oocytes among four to five experiments. (C) AQP expression at the cell surface (*EXPcs*). Data are expressed as means ± SE among three to four experiments.

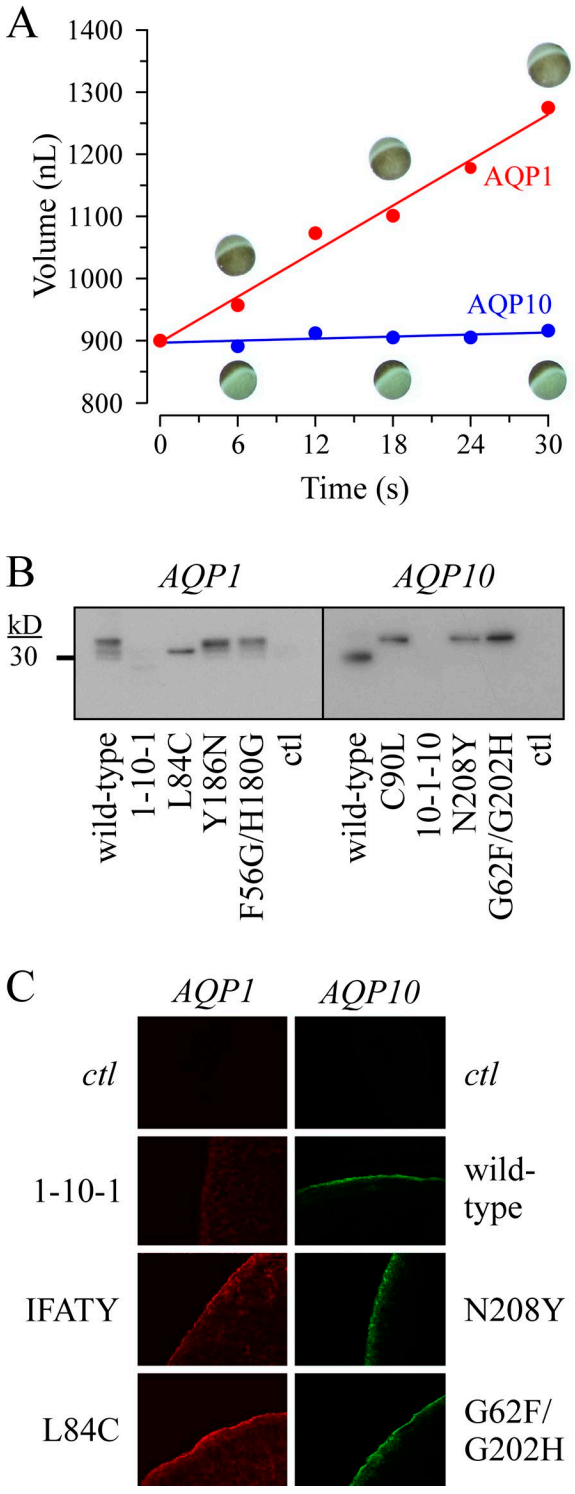

Figure 9. **Illustrative experiments.** (A) Water transport. After incubation in plain water, an oocyte expressing AQP1 and an oocyte expressing AQP10 were microphotographed at different time points for cell volume measurements. (B) Expression of wild-type and mutant AQPs by Western blot analyses. Samples correspond to cell surface proteins detected with an anti-AQP1 Ab (left) or an anti-AQP10 Ab (right). In each panel, water-injected oocytes were used as negative controls. (C) Immunofluorescence experiments. Cryosections postfixed in paraformaldehyde were obtained from AQP-expressing oocytes after a 3-d incubation in medium B1 at 18°C. Wild-type and mutant AQPs were detected with an anti-AQP1 Ab (left) or an anti-AQP10 Ab (right). For each Ab, water-injected oocytes were used as negative controls. Micrographs were taken under confocal microscopy and are shown in the panel for some of the AQPs: (top left) water, (second left) $AQP1_{1\text{-}10\text{-}1}$, (third left) $AQP1_{LGRND\rightarrow IFATY}$, (bottom left) $AQP1_{L84C}$, (top right) water, (second right) wild-type AQP10, (third right) $AQP10_{N208Y}$, and (bottom right) $AQP10_{G62F/G202H}$. Note that each of the micrographs is ~300 µm in actual width.

placed singly in AQP1 or in AQP10, no changes in transport characteristics were observed (not depicted).

Illustrative experiments

Fig. 9 displays representative data from the transport and expression experiments. In Fig. 9 A, an AQP1-expressing oocyte and an AQP10-expressing oocyte are used as examples to show changes in cell volumes as a function of time after incubation in plain water; in Fig. 9 B, bands correspond to wild-type or mutant channels present at the cell surface; and in Fig. 9 C, signals correspond to wild-type and mutant carriers expressed in oocyte cryosections.

DISCUSSION

This study presents the first structure–function analysis of selectivity-specifying residues for Si movement by the mammalian AQPs. The approach used consisted of interchanging one or many residues between a predominantly water-permeating channel (AQP1) and a predominantly Si-permeating channel (AQP10) at positions of divergence between conventional AQPs and AQGPs but of conservation within each group of channels. It led to the observation that the residue composition of the XX/R filter is key in allowing or restricting Si movement. It has also led to the identification of two other residues that are at some distance from the constriction site but that still appear important in specifying substrate selectivity.

The XX/R filter of AQP1 is composed of residues F_{56}-H_{180} and that in AQP10 is composed of residues G_{62}-G_{202}. In this work, remarkably, when AQP1 was mutated through an F-H→G-G substitution, it acquired the ability of permeating Si quite robustly, and when AQP10 was mutated through a G-G→F-H substitution, it lost the ability to do so. In this regard, previous experiments have shown that the F-H combination causes the pore to be narrower than the G-G combination (Beitz et al., 2006). One could thus postulate that in either isoform, the G-G combination is associated with a wider pore, of at least 4.6 Å in diameter, through which the movement of H_4SiO_4 is allowed. This possibility would be consistent with the importance of size constraint mechanisms to achieve substrate selectivity (Wang et al., 2005; Beitz et al., 2006).

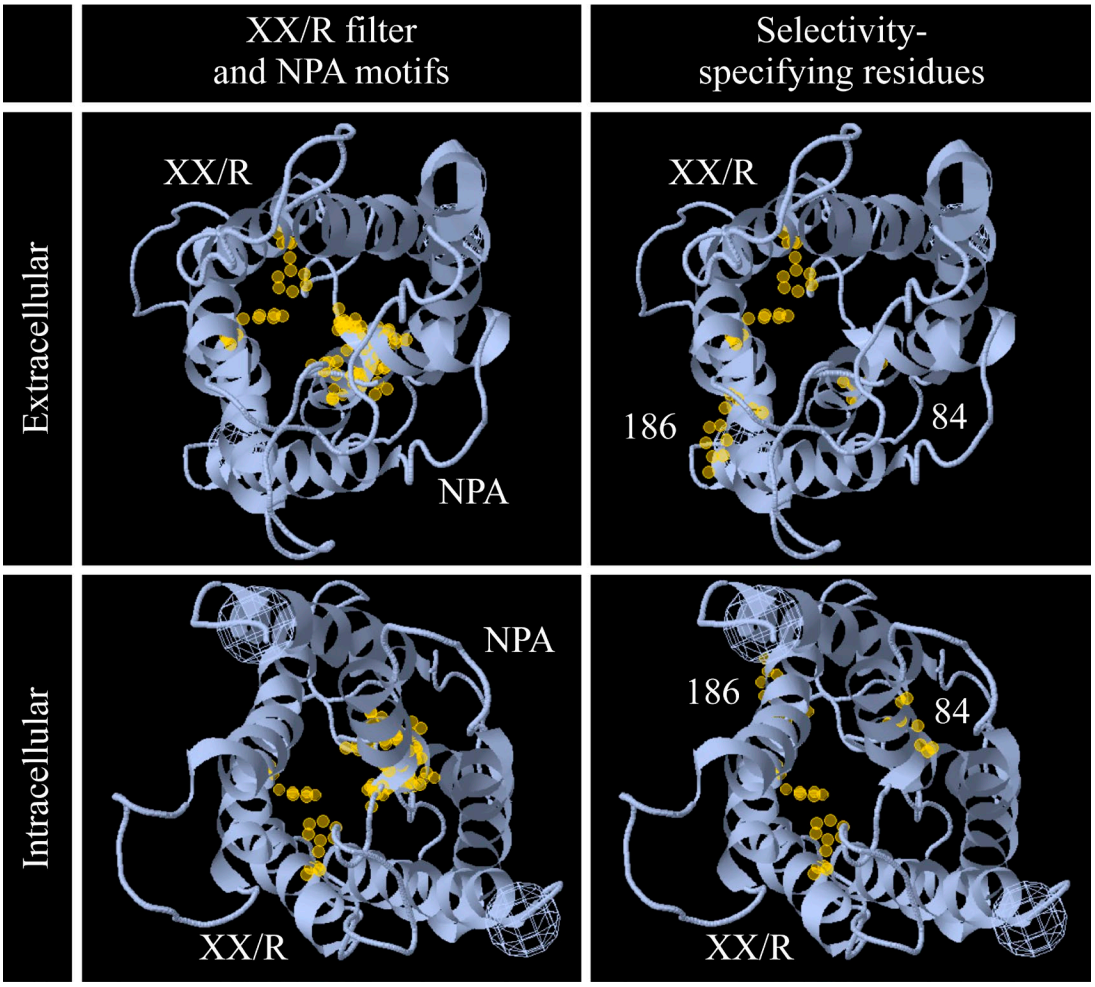

Figure 10. **Crystal structure of human AQP1.** The images were screen-printed from an open access database available at http://oca.weizmann.ac.il/oca-docs/fgij/fg.htm?mol=1FX8. The yellow circles correspond to carbon atoms within individual residues. The model was originally determined by Ren et al. (2000) at 3.70-Å resolution through electron crystallography of ice-embedded 2-D crystals.

Intriguingly, the composition of the XX/R filter did not appear to be important in conveying differences in water permeability between the two isoforms. In particular, our mutagenic experiments showed that AQP1 remained highly permeable to water even when residues F-H were replaced by residues G-G and that AQP10 remained almost impermeable to water even when residues G-G were replaced by residues F-H. In and of themselves, these results suggest that other sites in or near the pore region must play a role in determining water selectivity and that they would therefore include neither of the highly conserved NPA dipoles (Wu et al., 2009).

One of the sites that could play such a role in AQP1 was localized at position 84 and is occupied by a leucine residue, whereas the corresponding site in AQP10 is localized at position 90 and occupied by a cysteine residue. Indeed, we observed that L↔C substitutions at these positions led to substantial changes in water permeability—becoming much lower in AQP1 and much higher in AQP10—but to no changes in Si permeability. It should be mentioned, however, that the cysteine residue is conserved among all AQGPs, but that AQP9 in particular is known to exhibit higher permeability to water than AQP10 (Garneau et al., 2015). Hence, it is possible that water selectivity is specified through additional sites in or near the pore region.

If selectivity-specifying residues exist for water, the same must hold true for Si. Our experiments confirmed that this was probably the case and also showed that the site identified appeared to play little, if any, role in water permeability. This site is localized at position 208 in AQP10 and occupied by a tyrosine residue, whereas it is localized at position 186 in AQP1 and occupied by an asparagine residue. It should be mentioned here again that this residue is also highly conserved among the AQGPs but that AQP3 in particular exhibits much lower permeability to Si. As for water, hence, selectivity for Si must be specified through more than just one site in or near the pore region.

Based on the 2-D models of Fig. 10 and as already alluded to in Results, the carbon backbones, side chains,

or O_2 atoms of residues L_{84}/C_{90} and N_{186}/Y_{208} do not appear to be in close contact with the pore, XX/R filter, or NPA motifs. If this were the case, the sites where these residues are localized could still play a role in substrate coordination or selectivity if by affecting helix shape or spatial orientation they also affected pore diameter or organization. One must also remember that proteins tend to undergo many conformational transitions during their normal operation but that within growing crystal lattices they are often present in their single most prevalent and favorable structural state (Price, 2014). On average, hence, residues L_{84}/C_{90} and N_{186}/Y_{208} could lie much closer to the pore than expected from the proposed models of AQP1 and GlpF.

An obvious limitation of the approach used in this work to decipher mechanisms of substrate selectivity is that the residues involved will be missed if they are the same between AQP1 and AQP10. At the same time, it seems unlikely that such residues would be no more critical than the highly conserved NPA and R residues in ensuring proper channel function or that they would be physically very distant from the permeating unit. Another limitation of the approach exploited is that the substitutions generated could have induced long-range allosteric effects or rogue conformational transitions. In this study, reassuringly, many of the mutant channels were created through conservative substitutions and exhibited the hallmarks of functional AQPs.

In the light of previous data on the structural determinants of AQP function and of those presented in this work, it is tempting to propose an updated model of substrate movement through the water channel family. In this model, selectivity would be determined at multiples sites along the pore. One of these sites, the XX/R filter, would act as a barrier for restricting the movement of Si or substrates such as glycerol when the residue composition of XX causes the pore to be constricted at a diameter of <3.4 Å. The other sites, consisting of selectivity-specifying residues, would act as possible components of substrate-specific binding sites, thereby explaining why the restricted selectivity profiles of AQP family members cannot be solely accounted for by size constraint mechanisms.

In conclusion, we have demonstrated the importance of the XX/R filter in Si transport by the AQPs and have identified two additional residue sites that appear to play a key role in substrate selectivity. Our data therefore suggest that for this family of channels permeation through the pore is controlled by more than one restriction mechanism.

ACKNOWLEDGMENTS

The authors are grateful to Dr. Jean-Yves Lapointe from Montreal University for expert advice.

This study was supported by Canadian Institute of Health and Research (CIHR) grants. P. Isenring holds a CIHR-Chair in molecular physiology.

The authors declare no competing financial interests.
Sharona E. Gordon served as editor.

Submitted: 29 March 2016
Accepted: 18 July 2016

REFERENCES

Beitz, E., B. Wu, L.M. Holm, J.E. Schultz, and T. Zeuthen. 2006. Point mutations in the aromatic/arginine region in aquaporin 1 allow passage of urea, glycerol, ammonia, and protons. *Proc. Natl. Acad. Sci. USA.* 103:269–274. http://dx.doi.org/10.1073/pnas.0507225103

Bergeron, M.J., E. Gagnon, L. Caron, and P. Isenring. 2006. Identification of key functional domains in the C terminus of the K^+-Cl^- cotransporters. *J. Biol. Chem.* 281:15959–15969. http://dx.doi.org/10.1074/jbc.M600015200

Bienert, G.P., A.L. Møller, K.A. Kristiansen, A. Schulz, I.M. Møller, J.K. Schjoerring, and T.P. Jahn. 2007. Specific aquaporins facilitate the diffusion of hydrogen peroxide across membranes. *J. Biol. Chem.* 282:1183–1192. http://dx.doi.org/10.1074/jbc.M603761200

Braun, T., A. Philippsen, S. Wirtz, M.J. Borgnia, P. Agre, W. Kühlbrandt, A. Engel, and H. Stahlberg. 2000. The 3.7 Å projection map of the glycerol facilitator GlpF: a variant of the aquaporin tetramer. *EMBO Rep.* 1:183–189. http://dx.doi.org/10.1093/embo-reports/kvd022

Deshmukh, R.K., J. Vivancos, G. Ramakrishnan, V. Guérin, G. Carpentier, H. Sonah, C. Labbé, P. Isenring, F.J. Belzile, and R.R. Bélanger. 2015. A precise spacing between the NPA domains of aquaporins is essential for silicon permeability in plants. *Plant J.* 83:489–500. http://dx.doi.org/10.1111/tpj.12904

Gagnon, E., M.J. Bergeron, G.M. Brunet, N.D. Daigle, C.F. Simard, and P. Isenring. 2004. Molecular mechanisms of Cl^- transport by the renal Na^+-K^+-Cl^- cotransporter. Identification of an intracellular locus that may form part of a high affinity Cl^--binding site. *J. Biol. Chem.* 279:5648–5654. http://dx.doi.org/10.1074/jbc.M311218200

Gagnon, E., M.J. Bergeron, N.D. Daigle, M.H. Lefoll, and P. Isenring. 2005. Molecular mechanisms of cation transport by the renal Na^+-K^+-Cl^- cotransporter: structural insight into the operating characteristics of the ion transport sites. *J. Biol. Chem.* 280:32555–32563. http://dx.doi.org/10.1074/jbc.M505511200

Garneau, A.P., G.A. Carpentier, A.A. Marcoux, R. Frenette-Cotton, C.F. Simard, W. Rémus-Borel, L. Caron, M. Jacob-Wagner, M. Noël, J.J. Powell, et al. 2015. Aquaporins mediate silicon transport in humans. *PLoS One.* 10:e0136149. http://dx.doi.org/10.1371/journal.pone.0136149

Hachez, C., and F. Chaumont. 2010. Aquaporins: a family of highly regulated multifunctional channels. *Adv. Exp. Med. Biol.* 679:1–17. http://dx.doi.org/10.1007/978-1-4419-6315-4_1

Herrera, M., N.J. Hong, and J.L. Garvin. 2006. Aquaporin-1 transports NO across cell membranes. *Hypertension.* 48:157–164. http://dx.doi.org/10.1161/01.HYP.0000223652.29338.77

Holm, L.M., T.P. Jahn, A.L. Møller, J.K. Schjoerring, D. Ferri, D.A. Klaerke, and T. Zeuthen. 2005. NH_3 and NH_4^+ permeability in aquaporin-expressing *Xenopus* oocytes. *Pflugers Arch.* 450:415–428. http://dx.doi.org/10.1007/s00424-005-1399-1

Ishibashi, K., M. Kuwahara, Y. Gu, Y. Kageyama, A. Tohsaka, F. Suzuki, F. Marumo, and S. Sasaki. 1997. Cloning and functional expression of a new water channel abundantly expressed in the testis permeable to water, glycerol, and urea. *J. Biol. Chem.* 272:20782–20786. http://dx.doi.org/10.1074/jbc.272.33.20782

Ishibashi, K., S. Hara, and S. Kondo. 2009. Aquaporin water channels in mammals. *Clin. Exp. Nephrol.* 13:107–117. http://dx.doi.org/10.1007/s10157-008-0118-6

Jugdaohsingh, R., M.R. Calomme, K. Robinson, F. Nielsen, S.H. Anderson, P. D'Haese, P. Geusens, N. Loveridge, R.P. Thompson, and J.J. Powell. 2008. Increased longitudinal growth in rats on a silicon-depleted diet. *Bone.* 43:596–606. http://dx.doi.org/10.1016/j.bone.2008.04.014

Ma, J.F., K. Tamai, N. Yamaji, N. Mitani, S. Konishi, M. Katsuhara, M. Ishiguro, Y. Murata, and M. Yano. 2006. A silicon transporter in rice. *Nature.* 440:688–691. http://dx.doi.org/10.1038/nature04590

Murata, K., K. Mitsuoka, T. Hirai, T. Walz, P. Agre, J.B. Heymann, A. Engel, and Y. Fujiyoshi. 2000. Structural determinants of water permeation through aquaporin-1. *Nature.* 407:599–605. http://dx.doi.org/10.1038/35036519

Price, S.L. 2014. Predicting crystal structures of organic compounds. *Chem. Soc. Rev.* 43:2098–2111. http://dx.doi.org/10.1039/C3CS60279F

Ren, G., A. Cheng, V. Reddy, P. Melnyk, and A.K. Mitra. 2000. Three-dimensional fold of the human AQP1 water channel determined at 4 Å resolution by electron crystallography of two-dimensional crystals embedded in ice. *J. Mol. Biol.* 301:369–387. http://dx.doi.org/10.1006/jmbi.2000.3949

Rojek, A., J. Praetorius, J. Frøkiaer, S. Nielsen, and R.A. Fenton. 2008. A current view of the mammalian aquaglyceroporins. *Annu. Rev. Physiol.* 70:301–327. http://dx.doi.org/10.1146/annurev.physiol.70.113006.100452

Wang, Y., K. Schulten, and E. Tajkhorshid. 2005. What makes an aquaporin a glycerol channel? A comparative study of AqpZ and GlpF. *Structure.* 13:1107–1118. http://dx.doi.org/10.1016/j.str.2005.05.005

Wu, B., C. Steinbronn, M. Alsterfjord, T. Zeuthen, and E. Beitz. 2009. Concerted action of two cation filters in the aquaporin water channel. *EMBO J.* 28:2188–2194. http://dx.doi.org/10.1038/emboj.2009.182